Journal of Physics and Its Applications

Journal homepage : https://ejournal2.undip.ac.id/index.php/jpa/index

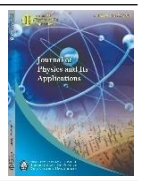

Optimizing Dose Distribution with Direct Aperture Optimization: A MatRad-Based Analysis

Fajar Miraz Fauzi, Siti Mutmainnah, Rio Rizky Rahmadani, and Freddy Haryanto*

Nuclear Physics and Biophysics Research Group, Faculty of Mathematics and Natural Sciences, Institut Teknologi Bandung, Bandung, Indonesia

**Corresponding author: freddy@itb.ac.id*

ARTICLE INFO

Article history:
Received: 17 November 2025
Accepted: 10 August 2026
Available online: 31 August 2026

Keywords:
Bixel
Direct Aperture Optimization
Dosimetry
MatRad
Treatment Planning System

ABSTRACT

Advanced optimization algorithms like Direct Aperture Optimization (DAO) are integral to modern radiotherapy, yet research is often hindered by the limited accessibility of commercial Treatment Planning Systems. Open-source platforms like matRad provide a vital framework for such investigations. This study evaluates the dosimetric impact of DAO activation and its interplay with varying bixel resolutions (5×5 to 10×10 mm^2) using matRad for a liver cancer case. Twelve treatment plans were generated and calculated using the ompMC Monte Carlo engine. Initial verification yielded a 3.14% mean relative statistical uncertainty, indicating that the stochastic uncertainty was relatively small compared with the dosimetric differences investigated. Twelve plans were assessed using Dose Volume Histograms (DVHs), Conformity Index (CI), and Homogeneity Index (HI). Results showed DAO significantly reduced stomach dose (e.g., 6.33% at 5×5 mm^2; p=0.031). At 5×5 mm^2, heart and liver mean doses decreased by 7.15% and 1.83% respectively, though these changes were resolution-dependent and statistically non-significant. For targets, DAO at 5×5 mm^2 caused minor, non-significant mean dose increases for the GTV (1.3%), CTV (1.01%), and PTV (0.77%). Conversely, while maintaining target coverage, DAO activation produced a statistically significant degradation in dose conformity and homogeneity across all bixel sizes (p=0.031). These findings highlight an inherent optimization trade-off that DAO prioritizes steep dose gradients for maximal OAR protection at the expense of minor internal target dose heterogeneity. This study establishes matRad as an effective environment for elucidating optimization behaviors in radiotherapy planning.

1. Introduction

A Treatment Planning System (TPS) constitutes a central component of modern radiotherapy, as it determines the spatial distribution of radiation dose delivered to a patient based on anatomical imaging and clinical prescription [1]. By optimizing beam configurations and dose distributions, a TPS aims to achieve adequate target dose coverage while minimizing radiation exposure to surrounding healthy tissues and organs at risk (OARs) [2]. As radiotherapy techniques continue to evolve in complexity, advanced optimization and computational algorithms within TPS becomes increasingly critical in ensuring treatment efficacy and safety [3].

Optimization algorithms embedded in TPS play a decisive role in achieving high quality treatment plans [4]. In Intensity Modulated Radiation Therapy (IMRT), conventional inverse planning commonly employs Fluence Map Optimization (FMO), in which idealized fluence maps are first optimized and subsequently converted into deliverable multileaf collimator (MLC) apertures [5]. This two-step approach may introduce differences between the optimized fluence distribution and the dose distribution associated with the final deliverable apertures [4]. Direct Aperture Optimization (DAO) addresses this issue by incorporating deliverable MLC aperture parameters directly into the optimization process, thereby reducing the separation between optimization and treatment delivery [6,7].

DAO has been investigated extensively in radiotherapy treatment planning and has been reported to influence target dose conformity, OAR sparing, and other plan-quality characteristics [4,8]. However, the behavior and performance of DAO may depend on the optimization configuration, including the spatial resolution of the fluence or beamlet representation [4]. Bixel size determines the spatial resolution at which beam intensity is optimized and therefore represents an important planning parameter that may affect the balance between dose modulation flexibility, plan quality, and computational requirements [9,10]. Consequently, systematic evaluation of DAO across different bixel resolutions is important for understanding whether the dosimetric effects attributed to DAO remain consistent under different optimization conditions.

Despite the extensive investigation of DAO in commercial treatment planning systems, research on treatment planning optimization remains constrained by the proprietary nature of many commercial TPS platforms. High licensing costs, closed-source architectures, and limited access to underlying optimization algorithms can restrict the ability of academic researchers to systematically investigate and modify treatment planning methodologies [11–13]. These limitations are particularly relevant for methodological studies in which researchers seek to isolate the effects of individual optimization parameters or develop extensions to existing algorithms.

To address these limitations, open source TPS platforms such as matRad have emerged as transformative tools in radiotherapy research. Developed by Wieser et al. [3], matRad offers a MATLAB based framework that supports a broad spectrum of treatment modalities, including IMRT [3]. Its modular design allows researchers to access and modify core algorithms for dose calculation and plan optimization. The transparent and customizable architecture of matRad facilitates experimentation with advanced methods such as DAO, which would otherwise remain inaccessible in commercial TPS environments [1,3,14].

Although DAO itself is not a new optimization concept and has been extensively investigated in commercial TPSs, the systematic characterization of DAO-related dosimetric changes across different bixel resolutions within an open-source TPS remains relevant for treatment planning research and education. In particular, it is important to determine whether the potential OAR-sparing effects associated with DAO are consistent across different optimization resolutions and whether such changes are accompanied by alterations in target conformity and dose homogeneity. This controlled evaluation can provide insight into the interaction between DAO and optimization resolution while avoiding confounding effects from changes in beam arrangement or other planning parameters.

Therefore, this study evaluates the dosimetric impact of DAO in IMRT planning using the open-source matRad framework. DAO-enabled and non-DAO plans were systematically compared across bixel sizes ranging from 5×5 to 10×10 mm^2 while maintaining the same beam arrangement and other optimization parameters. Treatment plan quality was evaluated using OAR mean and maximum doses, target dose metrics, the Conformity Index (CI), and the Homogeneity Index (HI). Through this controlled comparison, the study aims to characterize the relationship between DAO activation, bixel resolution, OAR sparing, and target dose distribution, thereby providing a reproducible assessment of DAO behavior within an open-source treatment planning environment.

2. Method

2.1 Dataset and Structures

The study utilized a Digital Imaging and Communications in Medicine (DICOM) dataset representing a liver cancer case obtained from the matRad sample dataset. The dataset included predefined contours for the Planning Target Volume (PTV), Clinical Target Volume (CTV), Gross Tumor Volume (GTV), and adjacent organs at risk (OARs). The OARs evaluated in this study were the liver, duodenum, bowel, stomach, spinal cord, and heart. The use of these structures was based on their relevance to liver radiotherapy planning [15]. Because the present study was designed to systematically investigate the dosimetric effects of DAO and bixel resolution under controlled planning conditions, all treatment plans were generated for the same patient dataset.

2.2 Treatment Planning and Simulation Design

Treatment planning was performed using the open-source TPS matRad version 3.1.0. The treatment plans were generated using IMRT with five coplanar 6-MV photon beams positioned at gantry angles of 0°, 72°, 144°, 216°, and 288° [16], and utilized a constant 1000 mm Source to Axis Distance (SAD) for all beams, as illustrated in Fig. 1. This configuration was kept identical across all treatment plans to ensure that differences in dosimetric outcomes were primarily attributable to DAO activation and bixel resolution rather than changes in beam geometry.

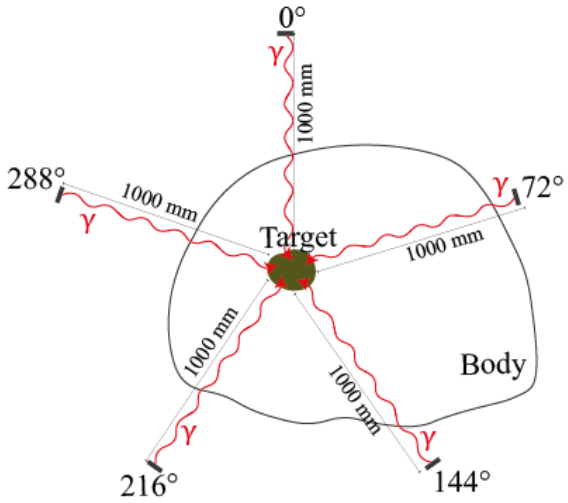

Fig. 1: Visualization of the beams gantry direction.

Two planning factors were investigated: bixel size and DAO activation. Six bixel sizes were evaluated, namely 5×5, 6×6, 7×7, 8×8, 9×9, and 10×10 mm^2. The selected range was based on previously reported beamlet resolutions used in treatment planning studies, including the use of a 5×5 mm^2 beamlet width for liver treatment planning [17] and beamlet widths within the range of 0.1–1.0 cm reported in previous TPS-based studies [18]. For each bixel size, two optimization conditions were generated: DAO enabled (DAO-on) and DAO disabled (DAO-off). This factorial combination resulted in 12 treatment plans, as summarized in Table 1.

Except for bixel size and DAO activation, all other treatment planning parameters were kept identical across the 12 plans. These parameters included the patient dataset, beam arrangement, photon energy, treatment prescription, optimization objectives and their corresponding weights, optimizer configuration, dose calculation settings, and other relevant planning parameters. Optimization was performed using the IPOPT optimizer. No additional user-defined MLC constraints were introduced or varied in this study, and MLC sequencing was not independently investigated. Dose distributions were calculated using the ompMC Monte Carlo dose engine integrated into matRad. The Monte Carlo calculation used 20,000 particle histories per beamlet. Depending on the spatial resolution, this resulted in a cumulative simulation of up to approximately 22.5 million total particle histories for a treatment plan with 1,125 bixels (e.g., 5×5 mm^2 resolution). Monte Carlo variance output was explicitly enabled, and dose error propagation was calculated to quantify the mean relative statistical uncertainty within the high-dose target region. The optimization objectives applied to the target volumes and OARs are summarized in Table 2.

Table 1: Simulation variation models

Models	Bixel Size (mm^2)	DAO Status (on/off)
Model 1	5×5	Off
Model 2	6×6	
Model 3	7×7	
Model 4	8×8	
Model 5	9×9	
Model 6	10×10	
Model 7	5×5	On
Model 8	6×6	
Model 9	7×7	
Model 10	8×8	
Model 11	9×9	
Model 12	10×10	

2.3 Dosimetric Evaluation

Each treatment plan was evaluated using dose distribution (isodose) maps, Dose Volume Histograms (DVHs), and quantitative dosimetric metrics. Isodose maps were used to qualitatively assess the spatial distribution of radiation dose within the target volumes. DVHs were generated to provide a quantitative representation of the relationship between absorbed dose and irradiated tissue volume for each target volume and OAR.

For the OARs, the mean absorbed doses were evaluated for the liver, stomach, heart, spinal cord, duodenum, and bowel. The resulting dose values were compared with published dose tolerance recommendations, particularly those reported by the Quantitative Analyses of Normal Tissue Effects in the Clinic (QUANTEC) [19]. These reference values were used to provide a clinical context for interpreting the dosimetric results rather than as absolute criteria for clinical treatment acceptance. In addition to the absolute dose values, the percentage difference between DAO-on and corresponding DAO-off plans was calculated to quantify the relative dosimetric change associated with DAO activation Target volume evaluation consisted of dose coverage, conformity, and homogeneity. The primary requirement was for adequate dose coverage, mandating that at least 95% of the target volume receives 95% of the prescribed dose (V95% ≥ 95%) [20]. Beyond coverage, the geometric quality of the plan was analyzed. Dose conformity was evaluated using the Conformity Index (CI), defined in the International Commission on Radiation Units and Measurements (ICRU) Report 62 as

$$CI = \frac{V_{IR}}{TV} \quad (1)$$

where V_{IR} is the volume covered of reference dose (95% prescribed dose), and TV is the target volume. A CI value of 1 represents ideal conformity according to the adopted criterion from Radiation Therapy and Oncology Group (RTOG) guidelines [21–23].

Furthermore, dose homogeneity within the target was quantified using the Homogeneity Index (HI), defined as the ratio of the maximum isodose (Imax) to the reference isodose (RI) [24].

$$HI = \frac{I_{max}}{RI} \quad (2)$$

A plan is considered compliant if the HI is ≤ 2, while values between 2 and 2.5 are considered minor violations, and those exceeding 2.5 are major violations, which may still be clinically acceptable in certain scenarios [24–26].

2.4 Statistical Analysis

The Wilcoxon signed-rank test was used to evaluate differences between DAO-on and DAO-off plans. The test was applied to the evaluated OAR dose parameters, including mean doses, as well as the CI and HI values of the target volumes.

Six paired observations were included in each statistical comparison, corresponding to the six investigated bixel sizes (5×5, 6×6, 7×7, 8×8, 9×9, and 10×10 mm^2). A two-sided p-value <0.05 was considered statistically significant [27]. The statistical analysis was performed using Python 3.11.

3. Results and Discussions

Prior to evaluating the dosimetric impact of DAO and bixel resolution, the statistical precision of the ompMC calculation was verified. Analysis of the extracted variance matrix demonstrated that the mean relative statistical uncertainty within the target volume was 3.14%. This value provides an estimate of the statistical precision of the Monte Carlo dose calculation and indicates that the stochastic uncertainty was relatively small compared with the magnitude of the dosimetric differences investigated [20].

Table 2: Optimization objectives, objective functions, weights, and dose parameters used for all treatment plans [19].

VOI	Type	Objective	Function	Weight (p)	Parameter
GTV	Target	1	Squared Deviation	1	$d_{ref} = 60$
CTV	Target	1	Squared Deviation	1	$d_{ref} = 60$
PTV	Target	1	Squared Deviation	1000	$d_{ref} = 60$
Stomach	OAR	2	Squared Overdose	1	$d_{max} = 45$
Duodenum	OAR	2	Squared Overdose	1	$d_{max} = 15$
Bowel	OAR	2	Squared Overdose	1	$d_{max} = 30$
Liver	OAR	2	Squared Overdose	1	$d_{max} = 42$
Heart	OAR	2	Squared Overdose	1	$d_{max} = 20$
Spinal Cord	OAR	2	Squared Overdose	1	$d_{max} = 45$

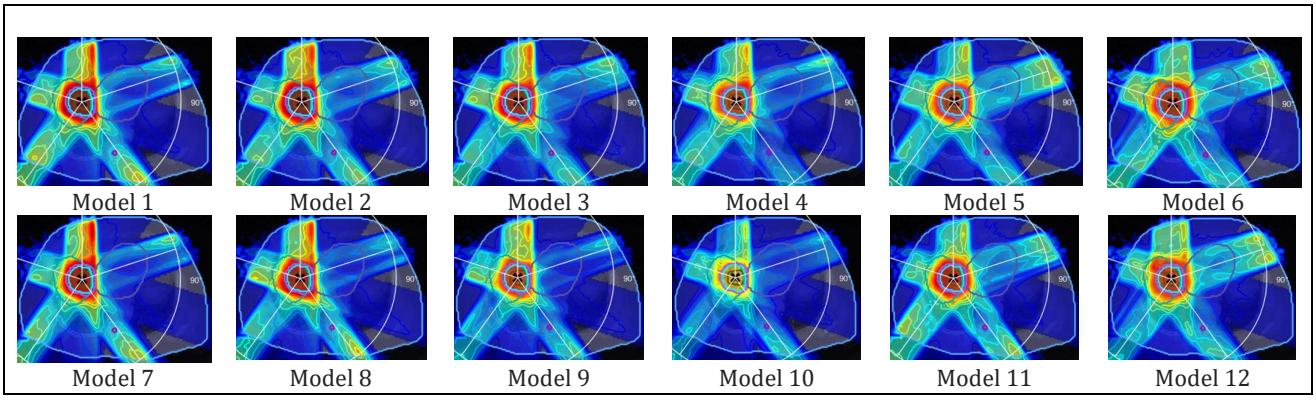

Fig. 2: Results of isodose maps in all simulation models.

3.1 Isodose Maps

A qualitative comparison of the isodose maps (shown in Fig. 2) revealed systematic differences associated with both bixel resolution and DAO activation. For the DAO-off plans (Models 1–6), increasing the bixel size from 5×5 to 10×10 mm^2 resulted in a progressively less detailed dose distribution and a shallower dose gradient around the target. This was visually evidenced by a reduced color gradation in the heatmap, characterized by a fading intensity of the high dose (deep red) region. Similarly, the models utilizing DAO-on (Models 7-12) also exhibited the same trend, wherein a larger bixel width resulted in a correspondingly shallower gradient. This direct relationship between a smaller bixel size and dose distribution aligns with the principle described by Sundström [28], that bixel size fundamentally determines the spatial resolution of the calculation grid, which in turn dictates the accuracy and detail of the resulting dose distribution.

The influence of DAO activation is clearly evident when comparing pairs of models with identical bixel sizes, such as Model 1 (5×5 mm^2, DAO-off) and Model 7 (5×5 mm^2, DAO-on). While the overall isodose shapes appear superficially similar, a detailed inspection of the high dose region, as shown in Fig. 3, reveals critical differences. The DAO-off plan (Model 1) produces a broader and more uniform peak dose (deep red) area within the PTV. However, this high dose region exhibits significant spillage outside the PTV contour. Meanwhile, the DAO-on plan (Model 7) appears to create a more minimal dose spillage beyond the PTV. This improvement, however, is accompanied by a reduction in dose homogeneity within the target volume, evidenced by the presence of lower dose areas (lighter red) inside the PTV. These dosimetric differences between active and inactive DAO plans become even more pronounced at coarser bixel resolutions, as observed in the subsequent model pairs (Model 2 vs. 8, through to Model 6 vs. 12). This aligns with the foundational work by Shepard et al. [29], which established that DAO is designed to produce highly conformal plans by directly optimizing beam apertures, a process which inherently alters and improves the resulting isodose map.

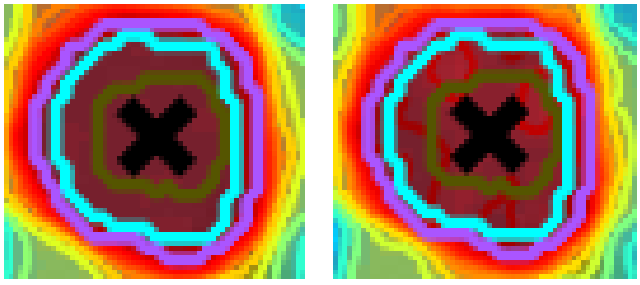

Fig. 3: Comparison of target volume dose distribution in model 1 (a) and model 7 (b).

3.2 Quantitative Dosimetric Analysis

3.2.1 Organs at Risk (OARs)

A quantitative analysis was performed based on dosimetric data extracted from the DVH. This evaluation aimed to objectively assess the quality of each treatment plan against established clinical criteria. Overall, All 12 simulation models satisfied the predefined dosimetric constraints evaluated in this study, wherein the dose received by all OARs was below the tolerance limits recommended by the QUANTEC guidelines.

For the liver, the mean dose limit is below 30-32 Gy (1 Gy/fraction). Model 7 (5×5 mm^2, DAO-on) recorded the lowest mean dose of 0.3606 Gy/fraction, while Model 5 (9×9 mm^2, DAO-off) recorded the highest at 0.4609 Gy/fraction. Activating DAO with the finest bixel resolution was able to reduce the mean dose to the liver by 21.76% compared to the with the highest mean liver dose observed among the DAO-off plans. When plans with identical bixel sizes were compared, DAO generally reduced the liver mean dose. For bixel resolutions ranging from 5×5 mm^2 to 9×9 mm^2, DAO activation consistently resulted in a reduction of the mean dose to the liver. The reduction varied across the resolutions: 1.83% at 5×5 mm^2, 0.63% at 6×6 mm^2, 2.07% at 7×7 mm^2, and 0.94% at 9×9 mm^2, with the most significant dose reduction of 6.69% occurring at the 8×8 mm^2 bixel size. Intriguingly, a contrary result was observed at the coarsest resolution of 10×10 mm^2, where DAO activation led to a minor mean dose increase of 1.33% compared to its non-DAO counterpart. Despite the generally lower liver dose with DAO, the difference between DAO-on and DAO-off plans was not statistically significant ($W = 4$, $p = 0.21975$). This result suggests a potential trade off in the optimization process at low spatial resolutions. It is plausible that to achieve a highly conformal dose distribution within the target volume with large, indivisible bixels, the DAO algorithm prioritizes target coverage and sparing of more critical serial organs, accepting a marginal dose increase in an adjacent, large parallel organ like the liver. This interpretation is supported by the principle that a reduction in IMRT plan complexity, such as that imposed by a coarser resolution, can significantly alter the quality of the final treatment plan [29]. At coarse resolutions, the optimizer's ability to generate a steep dose gradient between the target and a nearby OAR is limited. Consequently, even if high target conformality is achieved, a large adjacent organ may receive a slightly elevated dose as a result of this physical constraint [6,30].

A similar resolution-dependent behavior was observed for the heart. DAO reduced the mean heart dose by 7.15%, 5.46%, 6.99%, and 5.54% at 5×5, 6×6, 7×7, and 8×8 mm^2, respectively. However, this protective trend reversed at coarser resolutions. For the 9×9 mm^2 and 10×10 mm^2 bixels, DAO activation resulted in a slight increase in the mean dose by 0.1% and 2.95%, respectively, compared to their DAO-off counterparts. Overall, the activation of DAO did not yield a statistically significant reduction for the mean heart dose ($W = 3$, $p = 0.15625$). This phenomenon mirrors the observation for the liver and suggests a similar optimization trade off.

In contrast, the stomach showed the most consistent response to DAO. Activating DAO reduced the dose to the stomach in every paired comparison. The dose reduction was notably non-monotonic, ranging from a minimal 0.13% at the 7×7 mm^2 resolution to a substantial 14.88% at the 6×6 mm^2 bixel size. The specific reductions for the remaining bixel sizes were 6.33% (5×5 mm^2), 9.62% (8×8 mm^2), 3.43% (9×9 mm^2), and 3.88% (10×10 mm^2). Unlike the liver and heart, the reduction in mean stomach dose was statistically significant ($W = 0$, $p = 0.03125$), indicating a consistent dosimetric benefit of DAO for stomach sparing across the investigated bixel resolutions.

For the spinal cord, the DAO-off plans produced mean doses ranging from 0.1259 to 0.1554 Gy/fraction. In contrast, the corresponding DAO-on plans returned undefined (NaN) values for the mean dose statistics in the matRad DVH output. Therefore, these values should not be interpreted as an absolute dose of 0 Gy. The patient geometry, beam arrangement, and spinal cord contour were identical between the DAO-on and DAO-off plans, while only the DAO status was varied. Moreover, the measurable spinal cord dose in the corresponding DAO-off plans confirms that the spinal cord was included in the calculation geometry and was exposed to radiation. Because the DAO-on dose statistics were returned as NaN, they could not be treated as valid numerical measurements for paired statistical comparison. Accordingly, no Wilcoxon signed-rank test was performed for the spinal cord. The occurrence of NaN should therefore be regarded as a limitation of the reported dose-statistics output in the present matRad calculation rather than as evidence of complete absence of radiation dose.

The bowel and duodenum received zero reported dose across all 12 simulations, with the corresponding high-dose volume metrics also equal to zero. Because these values were unchanged by DAO activation or bixel resolution, they were not used to characterize the relative effect of DAO. Instead, they indicate that these structures received negligible dose within the present planning geometry and dose-calculation resolution. Accordingly, no statistical comparison was performed for these structures because there was no variation between the paired treatment plans.

3.2.2 Target Volumes

The analysis of the target volumes focused on dose coverage effectiveness, mean dose, conformity index, and homogeneity index. In terms of dose coverage, the V95% (volume received ≥ 95% prescribed dose) values in all models indicated that the target received adequate dose, with values approaching the prescribed 2 Gy/fraction. DAO activation did not show a uniform pattern of increasing or decreasing V95% but consistently maintained the values within a clinically acceptable range.

The impact of DAO activation on the mean dose delivered to the target volumes (PTV, CTV, and GTV) was found to be complex, resulting in minor but non-uniform modulations across the different bixel resolutions. A general trend was observed where DAO activation tended to slightly increase the mean dose at finer resolutions (5×5 mm^2 and 6×6 mm^2) but resulted in a slight dose reduction at most of the coarser resolutions. Specifically for the GTV, DAO activation led to a 1.3% dose increase with the 5×5 mm^2 bixel, whereas it produced a 1.52% dose reduction with the 10×10 mm^2 bixel. A similar pattern was noted for the PTV and CTV, with dose increases of 0.77% and 1.01% respectively at the 5×5 mm^2 size. For all other bixel sizes from 7×7 mm^2 to 10×10 mm^2, the changes were predominantly minor reductions, with the exception of a small 0.07% increase for the CTV at the 9×9 mm^2 resolution.

Statistical analysis confirmed that these minor modulations in mean dose resulting from DAO activation were not statistically significant for the GTV (W = 7, p = 0.5625), CTV (W = 9, p = 0.84375), and PTV (W = 6, p = 0.4375). These minor fluctuations, which were almost all within a ±1.5% margin, suggest that the primary function of the DAO algorithm is to reshape the dose distribution rather than to fundamentally alter the overall dose level delivered to the target. This finding is consistent with the study by Nguyen et al. [31], upon comparing two different DAO methods, found that while the dose distribution for OAR sparing and overall plan quality was improved, the mean PTV dose remained nearly identical between the methods. Furthermore, the work of Wu et al. [4] provides a mechanistic explanation for this stability. They describe that the stochastic nature of DAO can produce sub optimal MLC segments, particularly near the target/OAR boundary, and that a more detailed MLC leaf adjustment is required as a subsequent optimization step to eliminate hotspots or coldspots within the target. This implies that the core DAO process is not primarily designed for fine tuning the internal target dose. Consequently, the observed stability of the mean dose in this study is a logical outcome, demonstrating that DAO successfully optimizes the plan's spatial characteristics while preserving the intended therapeutic dose level.

3.3 Conformity and Homogeneity Indices

Dosimetric data extracted from the DVH were subsequently used to calculate the CI and HI. The results of these calculations for all models are presented in Table 3.

A detailed analysis of the conformity index reveals that DAO activation consistently resulted in slightly less ideal values (further from 1) compared to the DAO-off models at identical bixel resolutions. For instance, at the 5×5 mm^2 resolution, the CI value decreased from 0.9653 for the DAO-off model (Model 1) to 0.9623 for the DAO-on model (Model 7). This dosimetric shift is also reflected in the DVH curve, as shown in Fig. 4, where the PTV for Model 7 exhibits a shallower dose fall-off compared to Model 1, suggesting greater dose heterogeneity within the target. A lower CI value with DAO-on models was consistent across all evaluated bixel sizes, and statistical analysis confirmed that this systematic reduction in dose conformity was statistically significant (W = 0, p = 0.03125).

Table 3: CI and HI value for all models.

Models	CI Value	HI Value
Model 1	0.9653	1.0142
Model 2	0.9752	1.0241
Model 3	0.9829	1.0316
Model 4	0.9841	1.0278
Model 5	0.9878	1.0292
Model 6	0.9902	1.0292
Model 7	0.9623	1.0646
Model 8	0.9663	1.0581
Model 9	0.9745	1.0628
Model 10	0.9792	1.0688
Model 11	0.9795	1.0655
Model 12	0.9808	1.0860

However, this minor reduction in the CI value should not be interpreted as a degradation of plan quality. The standard CI is a simple geometric ratio of volumes and does not account for the steepness of the dose gradient outside the target [31,32]. It is plausible that the DAO algorithm achieves superior OAR sparing by creating a sharp dose fall off, which may slightly contract the 95% isodose volume, thus minimally impacting the CI ratio. This aligns with reviews on the subject, such as that by Feuvret et al. [25], which note that many conformity indices do not fully account for the irradiation of surrounding healthy tissues. Therefore, the observed small decrease in CI is likely a consequence of DAO's primary function to prioritize a steep and highly conformal dose gradient for OAR protection, a crucial characteristic not fully captured by this specific metric.

The evaluation of the homogeneity index revealed a similarly consistent trend, where DAO-on models consistently produced higher HI values, indicating a less uniform dose distribution within the target compared to their DAO-off counterparts. For example, at the 10×10 mm^2 resolution, the HI increased from 1.0292 (Model 6, DAO-off) to 1.0860 (Model 12, DAO-on). This systematic degradation in dose homogeneity across all DAO-on plans was also found to be statistically significant (W = 0, p = 0.03125). This quantitative result is a direct numerical validation of the qualitative observation from the isodose maps, where DAO-on plans exhibited small areas of lower dose (lighter red) within the PTV. This phenomenon exemplifies a classic optimization trade off. As described by Craft, et al. [33], the objectives in IMRT planning are often competing. This means that, in general, an improvement with respect to one objective can only be achieved at the expense of another objective. In

this context, the DAO algorithm appears to prioritize the objective of maximal OAR sparing at the expense of achieving perfect dose homogeneity within the target. This slight increase in dose inhomogeneity may therefore represent an acceptable trade-off when OAR sparing is prioritized, provided that target coverage and relevant clinical constraints remain satisfied.

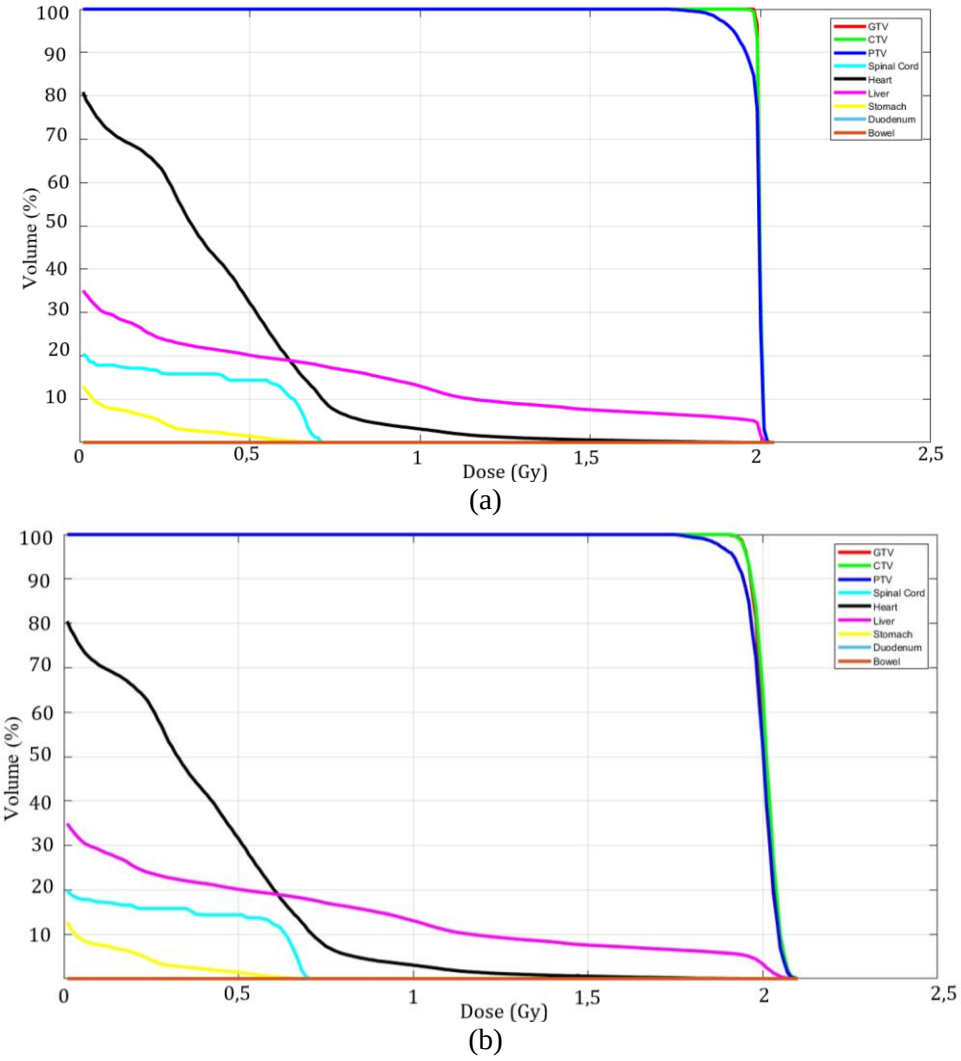

Fig. 4: Dose Volume Histogram for Model 1 (a) and Model 7 (b).

3.4 Clinical Implications and Study Limitations

From a clinical planning perspective, the appropriate balance between OAR sparing and target conformity or homogeneity depends on the specific treatment objective and institutional planning criteria. A modest reduction in conformity or homogeneity, as observed in the DAO-on plans, may be clinically acceptable when target coverage remains adequate and strict OAR constraints are satisfied. However, this study evaluated nominal dosimetric physical parameters only and did not incorporate Normal Tissue Complication Probability (NTCP) models. Therefore, the observed OAR dose reductions cannot be interpreted as direct evidence of reduced clinical toxicity. Future studies incorporating NTCP models and clinical outcome data are needed to determine whether these dosimetric improvements translate into clinically meaningful benefits.

The broader applicability of these findings must also be contextualized within the limitations of the study design. First, the analysis was based on a single liver cancer dataset to provide a controlled paired comparison. Thus, the absolute dosimetric values should not be generalized directly to other anatomical sites. Second, the evaluation was restricted to fixed-field photon IMRT using five coplanar beams. Consequently, the observed DAO-resolution relationship cannot be directly extrapolated to Volumetric Modulated Arc Therapy (VMAT) or proton therapy, which involve dynamic aperture modulation and different dose deposition characteristics. Third, the study did not investigate setup uncertainty, respiratory motion, or anatomical changes.

Finally, while the open-source matRad framework provides a transparent and reproducible environment, no direct benchmarking against a clinically commissioned commercial TPS (e.g.,

Eclipse, RayStation, or Monaco) was performed. Furthermore, treatment delivery metrics and computational efficiency, such as optimization time and specific monitor unit (MU) complexity, were outside the scope of this study. Future benchmarking efforts should incorporate these efficiency metrics alongside robustness analysis. Ultimately, the transparent architecture of matRad utilized in this study offers a foundational framework that can be extended to investigate multi-objective optimization, knowledge-based planning, and artificial intelligence-assisted treatment planning.

4. Conclusions

All simulation models satisfied the predefined dosimetric target coverage and OAR dose constraints evaluated in this study. The qualitative and quantitative analyses demonstrated that bixel resolution and DAO activation fundamentally influence the spatial dose distribution. While DAO activation provided statistically significant dose reductions for specific organs such as the stomach, its protective effect on large parallel organs like the liver and heart was highly resolution-dependent, performing optimally only at finer bixel sizes. For the target volumes, DAO preserved adequate dose coverage but introduced a statistically significant degradation in geometric conformity and dose homogeneity compared to DAO-off plans. This confirms a fundamental optimization trade-off inherent to the algorithm that DAO prioritizes the creation of steep dose gradients for critical OAR sparing at the expense of minor internal target dose heterogeneity.

The open-source matRad framework proved to be a robust computational environment for elucidating this nuanced interplay between optimization algorithms and beamlet resolution. To translate these dosimetric findings into clinical practice, future investigations should prioritize comparative benchmarking against commercially commissioned Treatment Planning Systems. Additionally, incorporating Normal Tissue Complication Probability (NTCP) models and evaluating plan robustness against setup uncertainties will be instrumental in bridging the gap between open-source academic research and clinical radiotherapy innovation.

Acknowledgments

The authors gratefully acknowledge the financial support for this research provided by the Indonesia Endowment Fund for Education (Lembaga Pengelola Dana Pendidikan, LPDP), Ministry of Finance of the Republic of Indonesia, and the Medical Physics Laboratory, Institut Teknologi Bandung (ITB), for providing computational resources and facilities that supported the computational work of this study.

References

[1] D. Sanchez-Parcerisa and J. Udías, "Teaching treatment planning for protons with educational open-source software: Experience with FoCa and MatRad," *J. Appl. Clin. Med. Phys.,* vol. 19, no. 4, pp. 302–306, 2018, doi: 10.1002/acm2.12326.

[2] L. Fu, P. Liu, X. Yang, L. Xiao, C. Long, Q. Liao, C. Mei, and J. Liu, "Dosimetric comparison of three sequential intensity-modulated radiotherapy planning methods in the Monaco system for postoperative left-sided breast cancer: A planning study," *J. Radiat. Res. Appl. Sci*., vol. 19, no. 1, p. 102103, 2026, doi: 10.1016/j.jrras.2025.102103.

[3] H. P. Wieser, N. Wahl, H. S. Gabryś, L. R. Müller, G. Pezzano, J. Winter, S. Ulrich, L. Burigo, O. Jäkel, and M. Bangert, "MatRad-an open-source treatment planning toolkit for educational purposes" *Med. Phys. Int. J.,* vol. 6, no. 1, pp. 119-127, 2018. [Online]. Available: http://mpijournal.org/pdf/2018-01/mpi-2018-01-p119.pdf. Accessed: Nov. 17, 2025.

[4] D. Wu, A. Eldib, L. Chen, and C. C. Ma, "MLC leaf adjustment for direct-aperture optimization treatment planning," *Mathews J. Cancer Sci.,* vol. 10, no. 1, p. 50, 2025, doi: 10.30654/mjcs.10050.

[5] Y. Zhang and M. Merritt, "Fluence map optimization in IMRT cancer treatment planning and a geometric approach," in Multiscale Optimization Methods and Applications, pp. 205–227, 2006, doi: 10.1007/0-387-29550-x_8.

[6] M. P. Milette and K. Otto, "Maximizing the potential of direct aperture optimization through collimator rotation," *Med. Phys.,* vol. 34, no. 4, pp. 1431–1438, 2007, doi: 10.1118/1.2712574.

[7] X. Zhu, T. Cullip, G. Tracton, X. Tang, J. Lian, J. Dooley, and S. X. Chang, "Direct aperture optimization using an inverse form of back-projection," *J. Appl. Clin. Med. Phys.,* vol. 15, no. 2, pp. 50–59, 2014, doi: 10.1120/jacmp.v15i2.4545.

[8] D. L. Craft, T. F. Halabi, H. A. Shih, and T. R. Bortfeld, "Approximating convex pareto surfaces in multiobjective radiotherapy planning," *Med. Phys.,* vol. 33, no. 9, pp. 3399–3407, 2006, doi: 10.1118/1.2335486.

[9] J. Markman, D. A. Low, A. W. Beavis, and J. O. Deasy, "Beyond bixels: generalizing the optimization parameters for intensity modulated radiation therapy," *Med. Phys.,* vol. 29, no. 10, pp. 2298–2304, 2002, doi: 10.1118/1.1508799.

[10] G. Redler, E. Pearson, X. Liu, I. Gertsenshteyn, B. Epel, C. Pelizzari, B. Aydogan, R. Weichselbaum, H. J. Halpern, and R. D. Wiersma, "Small animal IMRT using 3D-printed compensators" *Int. J. Radiat. Oncol. Biol. Phys.,* vol. 110, no. 2, pp. 551-565, 2021, doi: 10.1016/j.ijrobp.2020.12.028.

[11] ESTRO, "Resource sharing: Open-source software & development in radiotherapy." [Online]. Available: https://www.estro.org/Workshops/ESTRO-

Physics-Workshop-2024/Resource-sharing-open-source-software-development. Accessed: Nov. 17, 2025.

[12] N. Wahl, "Introduction to MatRad," presentation, 2022. [Online]. Available: https://indico.cern.ch/event/1161021/contributions/4876552/attachments/2475998/4249768/matRad_Introduction.pdf. Accessed: Nov. 17, 2025.

[13] S. Wuyckens, D. Dasnoy, G. Janssens, V. Hamaide, M. Huet, E. L. Lo¨yen, G. Rotsart De Hertaing, B. Macq, E. Sterpin, J. Lee, K. Souris, and S. Deffet, "OpenTPS -- Open-source treatment planning system for research in proton therapy," *arXiv preprint arXiv:2303.00365*, 2023. [Online]. Available: https://arxiv.org/abs/2303.00365. Accessed: Nov. 17, 2025.

[14] MathWorks, "Developing MatRad, an open-source dose calculation and optimization toolkit for radiation therapy planning." [Online]. Available: https://uk.mathworks.com/company/technical-articles/developing-matrad-an-open-source-dose-calculation-and-optimization-toolkit-for-radiation-therapy-planning.html. Accessed: Nov. 17, 2025.

[15] R. Michel, I. Françoise, P. Laure, M. Anouchka, P. Guillaume, and K. Sylvain, "Dose to organ at risk and dose prescription in liver SBRT," *Rep. Pract. Oncol. Radiother.,* vol. 22, no. 2, pp. 96–102, 2017, doi: 10.1016/j.rpor.2017.03.001.

[16] S. H. Kim, M. K. Kang, J. W. Yea, S. K. Kim, J. H. Choi, and S. A. Oh, "The impact of beam angle configuration of intensity-modulated radiotherapy in the hepatocellular carcinoma," *Radiat. Oncol. J.,* vol. 30, no. 3, pp. 146-151, 2012, doi: 10.3857/roj.2012.30.3.146.

[17] N. Khaledi, C. Hayes, L. Belshaw, M. Grattan, R. Khan, and J. L. Gräfe, "Treatment planning with a 2.5 MV photon beam for radiation therapy," *J. Appl. Clin. Med. Phys.,* vol. 23, no. 12, p. e13811, 2022, doi: 10.1002/acm2.13811.

[18] M. Wu, J. Jin, Z. Li, F. Kong, Y. He, L. Liu, W. Yang, and X. Xu, "Influence of beamlet width on dynamic IMRT plan quality in nasopharyngeal carcinoma," *PeerJ*, vol. 10, p. e13748, 2022, doi: 10.7717/peerj.13748.

[19] L. B. Marks, E. D. Yorke, A. Jackson, R. K. Ten Haken, L. S. Constine, A. Eisbruch, S. M. Bentzen, J. Nam, and J. O. Deasy, "Use of normal tissue complication probability models in the clinic," *Int. J. Radiat. Oncol. Biol. Phys.,* vol. 76, no. 3, suppl., pp. S10-S19, 2010, doi: 10.1016/j.ijrobp.2009.07.1754.

[20] E. Y.-H. Chuang, C.-H. Hsieh, P.-W. Shueng, C.-X. Hsu, D.-Y. Kuo, Y.-F. Lu, H.-P. Yeh, and P.-Y. Hou, "Accelerated partial breast irradiation delivered with helical tomotherapy: Dosimetry and volumetric predictors of ipsilateral breast dose," *Cancers*, vol. 18, no. 13, p. 2122, 2026, doi: 10.3390/cancers18132122.

[21] International Commission on Radiation Units and Measurements (ICRU), "ICRU report 62: prescribing, recording and reporting photon beam therapy (supplement to ICRU report 50)." 1999. [Online]. Available: https://www.icru.org/report/prescribing-recording-and-reporting-photon-beam-therapy-report-62. Accessed: Nov. 17, 2025.

[22] W. Small, W. R. Bosch, M. M. Harkenrider, J. B. Strauss, N. Abu-Rustum, K. V. Albuquerque, S. Beriwal, C. L. Creutzberg, P. J. Eifel, B. A. Erickson, A. W. Fyles, C. L. Hentz, A. Jhingran, A. H. Klopp, C. A. Kunos, L. K. Mell, L. Portelance, M. E. Powell, A. N. Viswanathan, J. H. Yacoub, C. M. Yashar, K. A. Winter, and D. K. Gaffney, "NRG oncology/RTOG consensus guidelines for delineation of clinical target volume for intensity modulated pelvic radiation therapy in postoperative treatment of endometrial and cervical cancer: an update," *Int. J. Radiat. Oncol. Biol. Phys.,* vol. 109, no. 2, pp. 413–424, 2021, doi: 10.1016/j.ijrobp.2020.08.061.

[23] B. Goswami, R. K. Jain, S. Yadav, S. Kumar, S. Oommen, S. Manocha, and G. K. Jadhav, "A dosimetric study of volumetric arc modulation with rapidarc versus intensity-modulated radiotherapy in cervical cancer patients," *Journal of Clinical And Diagnostic Research,* vol. 15, no. 5, pp. XC01-XC05, 2021, doi: 10.7860/jcdr/2021/48635.14863.

[24] T. Kataria, K. Sharma, V. Subramani, K. Karrthick, and S. Bisht, "Homogeneity index: An objective tool for assessment of conformal radiation treatments," *J. Med. Phys.,* vol. 37, no. 4, pp. 207-213, 2012, doi: 10.4103/0971-6203.103606.

[25] L. Feuvret, G. Noël, J.-J. Mazeron, and P. Bey, "Conformity index: A review," *Int. J. Radiat. Oncol. Biol. Phys.*, vol. 64, no. 2, pp. 333–342, 2006, doi: 10.1016/j.ijrobp.2005.09.028.

[26] E. Shaw, R. Kline, M. Gillin, L. Souhami, A. Hirschfeld, R. Dinapoli, and L. Martin, "Radiation therapy oncology group: Radiosurgery quality assurance guidelines," *Int. J. Radiat. Oncol. Biol. Phys.,* vol. 27, no. 5, pp. 1231–1239, 1993, doi: 10.1016/0360-3016(93)90548-A.

[27] S. Kwak, "Are only *p*-values less than 0.05 significant? A *p*-value greater than 0.05 is also significant!," *J. Lipid Atheroscler.,* vol. 12, no. 2, pp. 89-95, 2023, doi: 10.12997/jla.2023.12.2.89.

[28] J. Sundström, "Scenario dose calculation for robust optimization in proton therapy treatment planning," *Master's thesis, Lund University, Sweden,* 2021, [Online]. Available: https://lup.lub.lu.se/student-papers/search/publication/9059444.

[29] D. M. Shepard, M. A. Earl, X. A. Li, S. Naqvi, and C. Yu, "Direct aperture optimization: A turnkey solution for step-and-shoot IMRT," *Med. Phys*., vol. 29, no. 6, pp. 1007–1018, 2002, doi: 10.1118/1.1477415.

[30] M. Broderick, M. Leech, and M. Coffey, "Direct aperture optimization as a means of reducing the complexity of intensity modulated radiation therapy plans," *Radiation Oncology,* vol. 4, p. 8, 2009, doi: 10.1186/1748-717x-4-8.

[31] D. Nguyen, D. O'Connor, D. Ruan, and K. Sheng, "Deterministic direct aperture optimization using multiphase piecewise constant segmentation," *Med. Phys*., vol. 44, no. 11, pp. 5596–5609, 2017, doi: 10.1002/mp.12529.

[32] I. Paddick, "A simple scoring ratio to index the conformity of radiosurgical treatment plans. Technical note," *J. Neurosurg.,* vol. 93, suppl. 3, pp. 219–222, 2000, doi: 10.3171/jns.2000.93.supplement.

[33] D. Craft, P. Süss, and T. Bortfeld, "The tradeoff between treatment plan quality and required number of monitor units in intensity-modulated radiotherapy," *Int. J. Radiat. Oncol. Biol. Phys.,* vol. 67, no. 5, pp. 1596–1605, 2007, doi: 10.1016/j.ijrobp.2006.11.034.